

# Nonhelical inverse transfer of a decaying turbulent magnetic field

Axel Brandenburg,<sup>1,2,\*</sup> Tina Kahniashvili,<sup>3,4,5,†</sup> and Alexander G. Tevzadze<sup>6,‡</sup>

<sup>1</sup>*Nordita, KTH Royal Institute of Technology and Stockholm University, Roslagstullsbacken 23, 10691 Stockholm, Sweden*

<sup>2</sup>*Department of Astronomy, AlbaNova University Center, Stockholm University, 10691 Stockholm, Sweden*

<sup>3</sup>*The McWilliams Center for Cosmology and Department of Physics,*

*Carnegie Mellon University, 5000 Forbes Ave, Pittsburgh, PA 15213, USA*

<sup>4</sup>*Department of Physics, Laurentian University, Ramsey Lake Road, Sudbury, ON P3E 2C, Canada*

<sup>5</sup>*Abastumani Astrophysical Observatory, Ilia State University,*

*3-5 Cholokashvili Ave, Tbilisi, GE-0194, Georgia*

<sup>6</sup>*Faculty of Exact and Natural Sciences, Tbilisi State University, 1 Chavchavadze Ave., Tbilisi, 0128, Georgia*

(Dated: July 29, 2014, Revision: 1.1 )

In the presence of magnetic helicity, inverse transfer from small to large scales is well known in magnetohydrodynamic (MHD) turbulence and has applications in astrophysics, cosmology, and fusion plasmas. Using high resolution direct numerical simulations of magnetically dominated self-similarly decaying MHD turbulence, we report a similar inverse transfer even in the absence of magnetic helicity. We compute for the first time spectral energy transfer rates to show that the inverse transfer is about half as strong as with helicity, but in both cases the magnetic gain at large scales results from velocity at similar scales interacting with smaller-scale magnetic fields. We argue that both inverse transfers are a consequence of the universal  $k^4$  and  $k^2$  subinertial range spectra for magnetic and kinetic energies, respectively. The shallower  $k^2$  spectrum forces the magnetic field to attain larger-scale coherence. The inertial range shows a clear  $k^{-2}$  spectrum and is the first example of fully isotropic magnetically dominated MHD turbulence exhibiting weak turbulence scaling.

PACS numbers: 98.70.Vc, 98.80.-k

The nature of magnetohydrodynamic (MHD) turbulence has received significant attention in recent years [1]. Whenever plasma is ionized, it is electrically conducting and Kolmogorov's turbulence theory [2] has to be replaced by an appropriate theory for MHD turbulence [3]. This becomes relevant under virtually all astrophysical circumstances. However, the universal character of MHD turbulence is debated and several fundamental questions remain unanswered: how do kinetic and magnetic energy spectra look like and are they similar? How does this depend on the magnetic Prandtl number,  $\text{Pr}_M = \nu/\eta$ , i.e., the ratio of kinematic viscosity and magnetic diffusivity? What is the role of the Alfvén effect, i.e., how does the presence of a finite Alfvén speed  $v_A$  enter the expression for the turbulent energy spectrum?

If the spectral properties of MHD turbulence are governed solely by the rate of energy transfer  $\epsilon$ , we know already from dimensional arguments that the spectrum must scale as  $E(k) \sim \epsilon^{2/3} k^{-5/3}$  with wavenumber  $k$ . However, MHD turbulence becomes increasingly anisotropic toward small scales [4], so the spectrum  $E(k_\perp, k_\parallel)$  depends on the wavenumbers perpendicular and parallel to the magnetic field  $\mathbf{B}$ , and is essentially given by  $\epsilon^{2/3} k_\perp^{-5/3}$ , so most of the energy cascades perpendicular to  $\mathbf{B}$ .

Over the past ten years, this model has received signif-

icant support from direct numerical simulations (DNS) [1, 5, 6]. This also applies to the case when the magnetic field is not imposed, but generated self-consistently by the turbulent velocity  $\mathbf{u}$  through dynamo action [7]. However, when  $\mathbf{B}$  is decaying, the result may be sensitive to initial conditions and depend on the ratio  $v_A/u_{\text{rms}}$  of root mean square (rms) Alfvén speed to rms turbulent velocity. Recent DNS [8] found numerical evidence for three different scalings: Iroshnikov–Kraichnan scaling [9] proportional to  $(\epsilon v_A)^{1/2} k^{-3/2}$  for  $v_A/u_{\text{rms}} = 0.9$ , Goldreich–Sridhar scaling [4] proportional to  $\epsilon^{2/3} k_\perp^{-5/3}$  for  $v_A/u_{\text{rms}} = 1.3$ , and weak turbulence scaling [10] proportional to  $(\epsilon v_A k_\parallel)^{1/2} k_\perp^{-2}$  for  $v_A/u_{\text{rms}} = 2.0$ ; see Ref. [11] for a comparison of these three scalings. However, their physical interpretation is subject to criticism in that dynamic alignment between  $\mathbf{u}$  and  $\mathbf{B}$  can be responsible for the shallower  $k^{-3/2}$  scaling [5] and the  $k^{-2}$  scaling could also be caused by a dominance of discontinuities [12].

It has usually been taken for granted that for non-helical turbulence, energy is cascading toward small scales. An inverse cascade has so far only been found for helical turbulence [3, 13] and was confirmed in DNS [14–16]. It is evident that this requires significant scale separation,  $k_0/k_1 \gg 1$ , where  $k_0$  is the wavenumber of the peak of the spectrum and  $k_1 = 2\pi/L$  is the minimal wavenumber of the domain of size  $L$ . Since an inverse transfer was not expected to occur in the absence of helicity, most previous work did not allow for  $k_0/k_1 \gg 1$ . However, when  $k_0/k_1$  is moderate, some inverse cascading was found [15]. The present work shows that this

---

\*Electronic address: brandenb@nordita.org

†Electronic address: tinatin@phys.ksu.edu

‡Electronic address: aleko@tevza.org

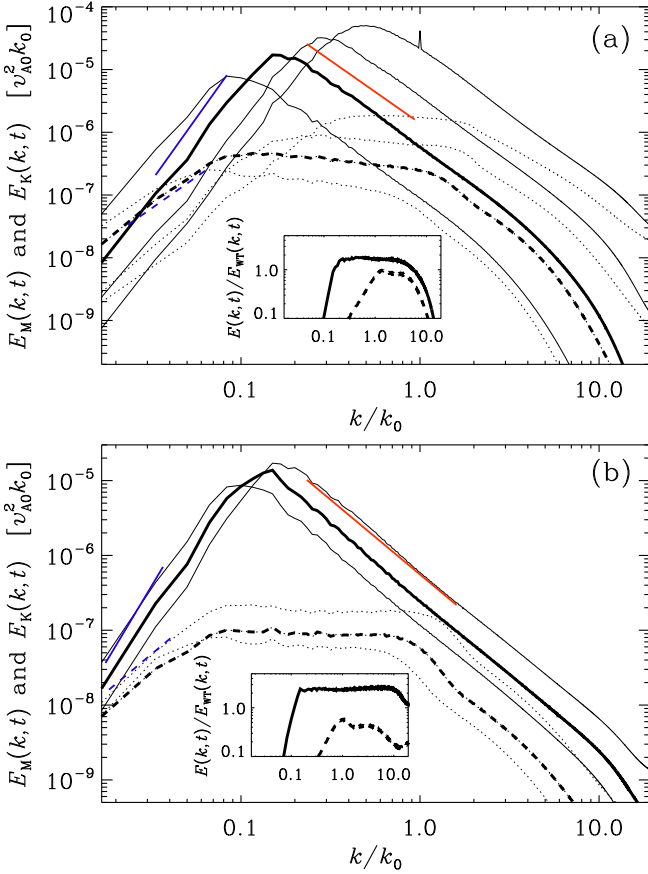


FIG. 1: (Color online) (a) Magnetic (solid lines) and kinetic (dashed lines) energy spectra for Run A at times  $t/\tau_A = 18, 130, 450$ , and  $1800$ ; the time  $t/\tau_A = 450$  is shown as bold lines. The straight lines indicate the slopes  $k^4$  (solid, blue),  $k^2$  (dashed, blue), and  $k^{-2}$  (red, solid). (b) Same for Run B, at  $t/\tau_A = 540, 1300$ , and  $1800$ , with  $t/\tau_A = 1300$  shown as bold lines. The insets show  $E_M$  and  $E_K$  compensated by  $E_{WT}$ .

behavior is genuine and more pronounced at higher resolution, larger Reynolds numbers and larger  $k_0/k_1$ .

We solve the compressible MHD equations for  $\mathbf{u}$ , the gas density  $\rho$  at constant sound speed  $c_s$ , and the magnetic vector potential  $\mathbf{A}$ , so  $\mathbf{B} = \nabla \times \mathbf{A}$ . Following our earlier work [17–19], we initialize our decaying DNS by restarting them from a snapshot of a driven DNS, where a random forcing was applied in the evolution equation for  $\mathbf{A}$  rather than  $\mathbf{u}$ . To allow for sufficient scale separation, we take  $k_0/k_1 = 60$ . We use the PENCIL CODE [20] at a resolution of  $2304^3$  meshpoints on 9216 processors. The code uses sixth order finite differences and a third order accurate time stepping scheme.

Our magnetic and kinetic energy spectra are normalized such that  $\int E_M(k,t) dk = \mathcal{E}_M(t) = v_A^2/2$  and  $\int E_K(k,t) dk = \mathcal{E}_K(t) = u_{rms}^2/2$  are magnetic and kinetic energies per unit mass. The magnetic integral scale is defined as  $\xi_M = k_M^{-1}(t) = \int k^{-1} E_M(k,t) dk / \mathcal{E}_M(t)$ . Time is given in initial Alfvén times  $\tau_A = (v_{A0} k_0)^{-1}$ , where

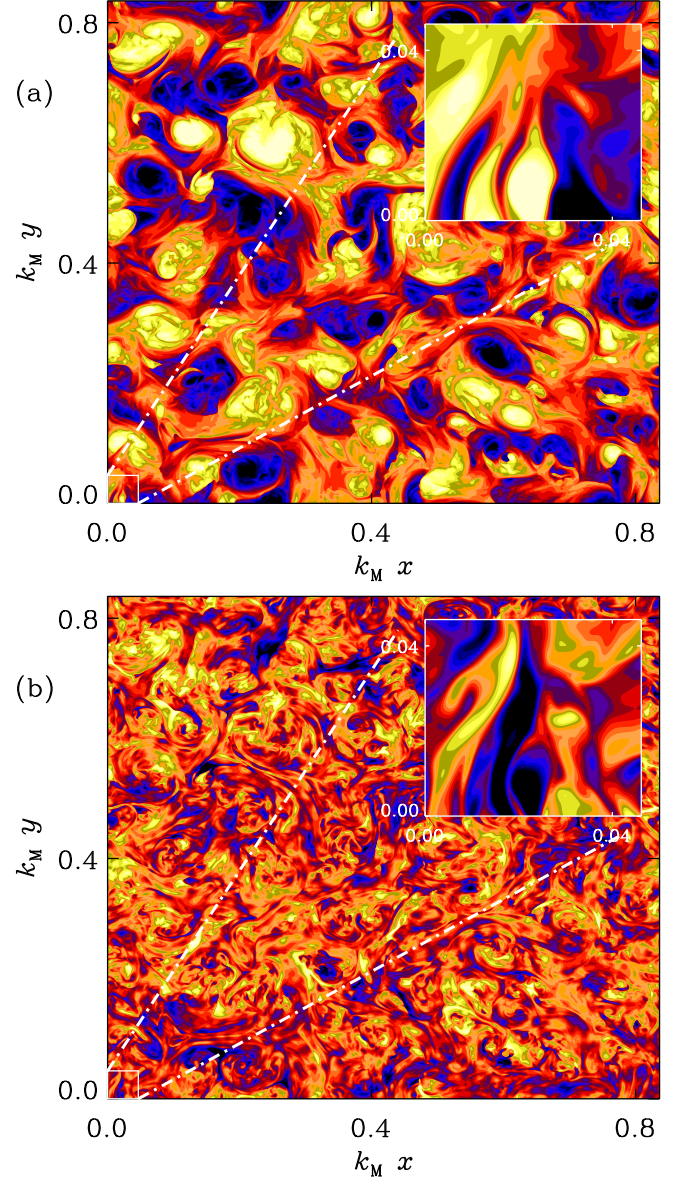


FIG. 2: (Color online) Contours of (a)  $B_z(x,y)$  and (b)  $u_z(x,y)$  for Run A. The insets show a zoom into the small square in the lower left corner.

$v_{A0} = v_A(0)$ . In Fig. 1 we show  $E_M(k,t)$  and  $E_K(k,t)$  for Runs A and B (restarted from A at  $t/\tau_A = 450$ ) with  $Pr_M = 1$  and  $10$ , respectively, and in Fig. 2 slices  $B_z(x,y)$  and  $u_z(x,y)$  at  $z = 0$  at the last time Run A. We find an inertial range with weak turbulence scaling,

$$E_{WT}(k,t) = C_{WT}(\epsilon v_A k_M)^{1/2} k^{-2}, \quad (1)$$

where  $k_M^{-1}(t) = \int k^{-1} E_M(k,t) dk / \mathcal{E}_M(t)$  is the integral scale and has been used in place of  $k_\parallel$ . The prefactor is  $C_{WT} \approx 1.9$  for  $Pr_M = 1$  and  $\approx 2.4$  for  $Pr_M = 10$ . In agreement with related work [3, 18],  $\mathcal{E}_M$  decays like  $t^{-1}$ .

At small wavenumbers the  $k^4$  and  $k^2$  subinertial ranges respectively for  $E_M(k,t)$  and  $E_K(k,t)$  are carried over

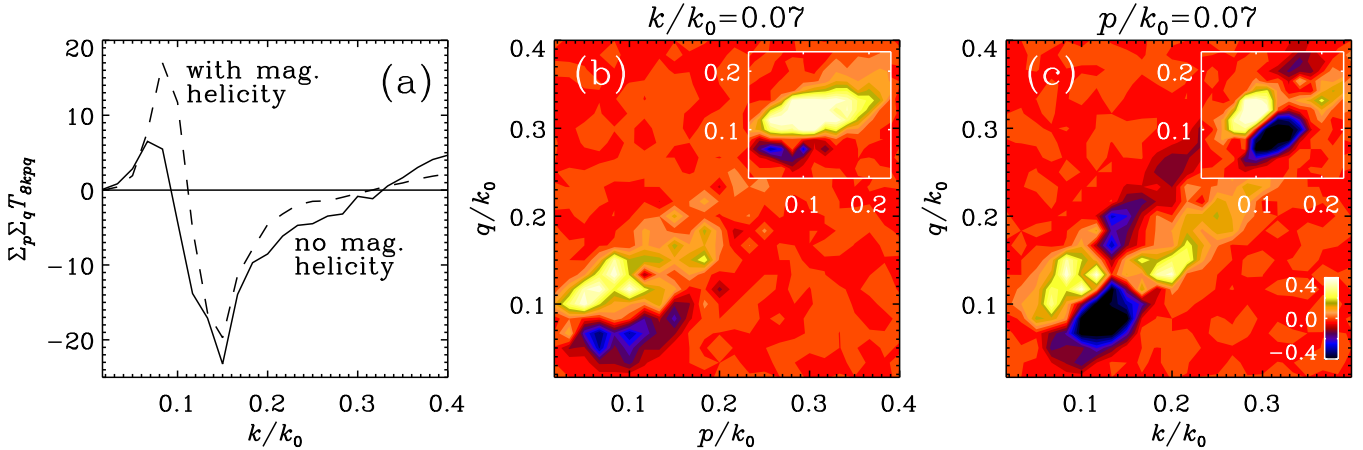


FIG. 3: (Color online) Spectral transfer function  $T_{kpq}$ , (a) as a function of  $k$  and summed over all  $p$  and  $q$ , (b) as a function of  $p$  and  $q$  for  $k/k_1 = 4$ , and (c) as a function of  $k$  and  $q$  for  $p/k_1 = 4$ . The dashed line in (a) and the insets in (b) and (c) show the corresponding case for a DNS with helicity; both for  $\text{Pr}_M = 1$ .

from the initial conditions. The  $k^4$  Batchelor spectrum is in agreement with the causality requirement [22, 23] for the divergence-free vector field  $\mathbf{B}$ , but for  $\mathbf{u}$  there is no zero-divergence requirement, allowing for the possibility of a white noise spectrum,  $E_K(k) \propto k^2$  [23]. The resulting difference in the scaling is also the reason that, even though magnetic energy dominates over kinetic, the two spectra must cross at sufficiently small wavenumbers. This idea may also apply to incompressible [24] and relativistic [25] simulations, where inverse nonhelical transfer has recently been confirmed.

To quantify the nature of inverse transfer we show in Fig. 3 representations of the spectral transfer function  $T_{kpq} = \langle \mathbf{J}^k \cdot (\mathbf{u}^p \times \mathbf{B}^q) \rangle$  and compare with the corresponding helical case of Ref. [19], but with  $1024^3$  mesh points and at a comparable time. Here, the superscripts indicate the radius of a shell in wavenumber space of Fourier filtered vector fields; see Ref. [16] for such an analysis in driven helical turbulence. The transfer function  $T_{kpq}$  quantifies the gain of magnetic energy at wavenumber  $k$  from interactions of velocities at wavenumber  $p$  and magnetic fields at wavenumber  $q$ . Fig. 3(a) shows a gain for  $k/k_0 < 0.1$ , which is about half of that for the helical case. The corresponding losses for  $k/k_0 > 0.1$  are about equal in the two cases. In both cases, the magnetic gain at  $k/k_0 = 0.07 = 4/60$  results from  $\mathbf{u}^p$  with  $0 < p/k_0 < 0.2$  interacting with  $\mathbf{B}^q$  at  $q/k_0 > 0.1$ ; see the light yellow shades in Fig. 3(b). Note that work done by the Lorentz force is  $\langle \mathbf{u}^p \cdot (\mathbf{J}^k \times \mathbf{B}^q) \rangle = -T_{kpq}$ . Thus, negative values of  $T_{kpq}$  quantify the gain of *kinetic* energy at wavenumber  $p$  from interactions of magnetic fields at wavenumbers  $k$  and  $q$ . Blue dark shades in Fig. 3(c) indicate therefore that the gain of kinetic energy at  $p/k_0 = 0.07$  results from magnetic interactions at wavenumbers  $k$  and  $q$  of around  $0.1 k_0$ . These results support the interpretation that the increase of spectral power at large scales is sim-

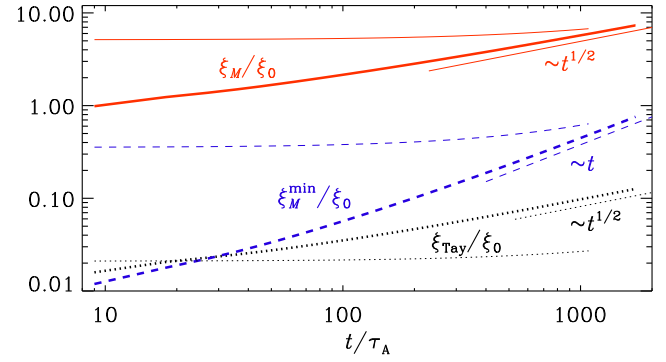


FIG. 4: Time evolution of  $\xi_M = k_M^{-1}$  and  $\xi_M^{\min}$ , as well as the Taylor microscale  $\xi_{\text{Tay}}$ . Fat (thin) lines are for Run A (B).

ilar to the inverse transfer in the helical case; see [26] for information concerning the total energy transfer.

To exclude that the inverse energy transfer is not a consequence of the invariance of magnetic helicity,  $\mathcal{H}_M(t) = \langle \mathbf{A} \cdot \mathbf{B} \rangle$ , we compare  $\xi_M$  with its lower bound  $\xi_M^{\min} = |\mathcal{H}_M|/2\mathcal{E}_M$  [18]; see Fig. 4. Even though the initial condition was produced with nonhelical plane waves, we find  $\mathcal{H}_M \neq 0$  due to fluctuations. Since  $\mathcal{H}_M$  is conserved and  $\mathcal{E}_M$  decays like  $t^{-1}$ ,  $\xi_M^{\min}$  grows linearly and faster than  $\xi_M \sim t^{1/2}$ , so they will eventually meet and then continue to grow as  $t^{-2/3}$  [3, 18].

During the course of the simulation, the gap between  $\xi_M$  and  $\xi_M^{\min}$  has shrunk from about two to one order of magnitude (Fig. 4). However, to close the gap completely and thus to reach a fully helical state that would explain inverse transfer, one would need to extend the simulation to  $t/\tau_A = 10^5$ . We have also verified that our turbulence is manifestly three-dimensional, eliminating therefore the possibility of an inverse cascade due to the invariance of  $\langle \mathbf{A}^2 \rangle$  in two dimensions [26].

TABLE I: Comparison of relative dissipation rates, energies and other parameters for the two simulations discussed.

Run	$\text{Pr}_M$	$v_{A0}/c_s$	$u_{\text{rms}}/v_A$	Lu	Re	$\epsilon_K/\epsilon_M$	$\epsilon_M/\epsilon$	$\epsilon_K/\epsilon$
A	1	0.15	0.36	700	230	0.52	0.66	0.34
B	10	0.03	0.21	6300	130	0.93	0.52	0.48

Since  $u_{\text{rms}}$ ,  $v_A$ , and  $k_M$  are all proportional to  $t^{-1/2}$  the decay is self-similar in such a way that the Reynolds and Lundquist numbers,  $\text{Re} = u_{\text{rms}}/\nu k_M$  and  $\text{Lu} = v_A/\eta k_M$ , remain constant. Since  $\mathcal{E}_K \ll \mathcal{E}_M$ , the dissipated energy comes predominantly from  $-d\mathcal{E}_M/dt$ , and yet a substantial fraction of it is used to drive kinetic energy by performing work on the Lorentz force. Nevertheless, the viscous to magnetic dissipation ratio  $\epsilon_K/\epsilon_M$  increases only by a factor of 1.8 as  $\text{Pr}_M$  increases from 1 to 10; see Table I. This is less than for kinetically driven MHD turbulence, where  $\epsilon_K/\epsilon_M \propto \text{Pr}_M^n$  with  $n = 0.3\text{--}0.7$  [27]. Therefore,  $\epsilon_M$  is here larger than in driven MHD turbulence, where large Lu can still be tolerated. This suggests that Run B may be under-resolved, which might also explain why it did not reach asymptotic scaling in Fig. 4.

In summary, we have shown that inverse transfer is a ubiquitous phenomenon of both helical and non-helical MHD. For helical MHD, this has been well known for nearly four decades [13], but for nonhelical MHD there have only been some low resolution DNS [15, 19]. Our high resolution DNS confirm the earlier hypothesis [19] that this inverse transfer is accomplished through small-scale magnetic field interacting with larger-scale velocity. At large enough length scales, kinetic energy always dominates over magnetic owing to the shallower  $k^2$  spectrum of kinetic energy, which we show is responsible for inverse transfer both in helical and nonhelical MHD. This is significant for cosmology and astrophysics [25], with applications not only to primordial magnetic fields, but also to ejecta from young stars, supernovae, and active galactic nuclei [28].

Our results confirm the existence of the weak turbulence  $k^{-2}$  scaling for a strong magnetic field that is here for the first time globally isotropic and not an imposed one [6]. The decay is slower than for equipartition strength MHD turbulence which is argued to be governed by the Loitsyansky invariant [21]. Future investigations of the differences between these types of turbulence are warranted. Interestingly, the extended plateau in the velocity spectrum around the position of the magnetic peak may be important for producing observationally detectable broad gravitational wave spectra [29].

We appreciate useful discussions with A. Neronov. Computing resources have been provided by the Swedish National Allocations Committee at the Center for Parallel Computers at the Royal Institute of Technology and by the Carnegie Mellon University Supercomputer Cen-

ter. We acknowledge support from the Swedish Research Council grants 621-2011-5076 and 2012-5797, the European Research Council AstroDyn Project 227952, the Research Council of Norway FRINATEK grant 231444, the Swiss NSF grant SCOPE IZ7370-152581, the NSF grant AST-1109180, and the NASA Astrophysics Theory Program grant NNX10AC85G. A.B. and A.T. acknowledge the hospitality of the McWilliams Center for Cosmology.

- 
- [1] W. H. Matthaeus, S. Ghosh, S. Oughton, and D. A. Roberts, *J. Geophys. Res.* **101**, 7619 (1996); J. Cho and E.T. Vishniac, *Astrophys. J.* **538**, 217 (2000); J. Maron and P. Goldreich, *Astrophys. J.* **554**, 1175 (2001).
  - [2] A. Kolmogorov, *Dokl. Akad. Nauk SSSR*, **30**, 301 (1941);
  - [3] D. Biskamp, *Magnetohydrodynamic Turbulence* (Cambridge: Cambridge Univ. Press) 2003.
  - [4] P. Goldreich and S. Sridhar, *Astrophys. J.* **438**, 763 (1995).
  - [5] J. Mason, F. Cattaneo, and S. Boldyrev, *Phys. Rev. Lett.* **97**, 255002 (2006).
  - [6] J.C. Perez and S. Boldyrev, *Astrophys. J. Lett.* **672**, L61 (2008).
  - [7] N. E. L. Haugen, A. Brandenburg, and W. Dobler, *Phys. Rev. E* **70**, 016308 (2004).
  - [8] E. Lee, M. E. Brachet, A. Pouquet, P. D. Mininni, D. Rosenborg, *Phys. Rev. E* **81**, 016318 (2010).
  - [9] R. S. Iroshnikov, *Sov. Astron.* **7**, 566 (1963); R. H. Kraichnan, *Phys. Fluids* **8**, 1385 (1965).
  - [10] S. Galtier, S.V. Nazarenko, A.C. Newell, and A. Pouquet, *J. Plasm. Phys.* **63**, 447 (2000).
  - [11] A. Brandenburg and Å. Nordlund, *Rep. Prog. Phys.* **74**, 046901 (2011).
  - [12] V. Dallas and A. Alexakis, *Astrophys. J.* **788**, L36 (2014).
  - [13] A. Pouquet, U. Frisch, and J. Léorat, *J. Fluid Mech.* **77**, 321 (1976).
  - [14] D. Balsara and A. Pouquet, *Phys. Plasmas* **6**, 89 (1999).
  - [15] M. Christensson, M. Hindmarsh, and A. Brandenburg, *Phys. Rev. E* **70**, 056405 (2001).
  - [16] A. Brandenburg, *Astrophys. J.* **550**, 824 (2001).
  - [17] T. Kahniashvili, A. Brandenburg, A. G. Tevzadze and B. Ratra, *Phys. Rev. D* **81**, 123002 (2010).
  - [18] A. G. Tevzadze, L. Kisslinger, A. Brandenburg and T. Kahniashvili, *Astrophys. J.* **759**, 54 (2012).
  - [19] T. Kahniashvili, A. G. Tevzadze, A. Brandenburg and A. Neronov, *Phys. Rev. D* **87**, 083007 (2013); note that in their Eq. (14),  $\mathbf{v}/\eta$  should read  $\partial\mathbf{v}/\partial\eta$ .
  - [20] <http://pencil-code.googlecode.com/>
  - [21] P. A. Davidson, *J. Turb.* **1**, 006 (2000).
  - [22] R. Durrer and C. Caprini, *JCAP* **0311**, 010 (2003).
  - [23] P. A. Davidson, *Turbulence* (Oxford Univ. Press, 2004).
  - [24] A. Berera and M. Linkmann, arXiv:1405.6756 (2014).
  - [25] J. Zrake, arXiv:1407.5626 (2014).
  - [26] See Supplemental Material in arXiv:1404.2238 for details.
  - [27] A. Brandenburg, *Astrophys. J.* **791**, 12 (2014).
  - [28] A. M. Beck, K. Dolag, H. Lesch, and P. P. Kronberg, *Mon. Not. R. Astron. Soc.* **435**, 3575 (2013).
  - [29] T. Kahniashvili, L. Campanelli, G. Gogoberidze, Y. Maravini, and B. Ratra, *Phys. Rev. D* **78**, 123006 (2008).

# Supplemental Material

**Abstract.** The subject of magnetically dominated decaying MHD turbulence has been addressed in several recent papers. The focus of the Letter [1] is the investigation of inverse transfer of magnetic energy at the expense of kinetic energy. In this Supplemental Material, we present additional properties of the resulting turbulence regarding the decay rate, the question of local two-dimensionality of the turbulence, and the spectral energy transfer functions.

## Initial condition

The simulations discussed in the Letter are motivated by applications to the early Universe such as the time of the electroweak phase transition. As shown in Ref. [2], the usual MHD equations can be applied with time  $t$  being replaced by the conformal time  $\tilde{t} = \int dt/R(t)$ , where  $R(t)$  is the scale factor in the assumed flat, isotropic, and homogeneous Universe being described by the Robertson-Walker metric.

Our goal is to have an initial condition that quickly leads to self-similar decay. Earlier experience [3–5] has shown that this is easily achieved by using a turbulence simulation that was driven with a stochastic monochromatic forcing in the equation for the magnetic vector potential. The initial condition used in our present work is shown in Fig. 5. It shows approximate  $k^2$  and  $k^4$  subinertial ranges for kinetic and magnetic energy spectra, respectively. Both spectra are maintained also at later times in such a way that they gradually shift upward with time (see Fig. 1 of the Letter).

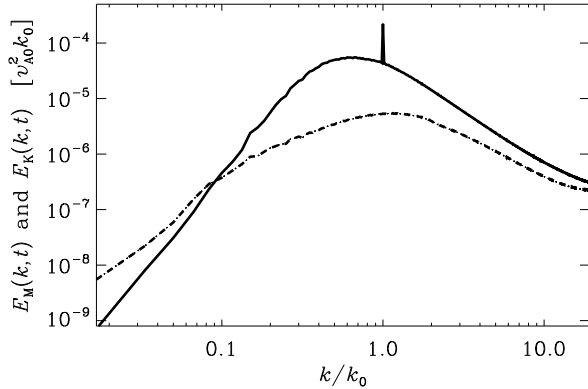


FIG. 5: Magnetic (solid lines) and kinetic (dashed lines) energy spectra for the initial condition of Run A.

In the present simulations (Run A of the Letter), both magnetic and kinetic energies show a slight uprise of power near the Nyquist wavenumber,  $k_{Ny} = \pi/\delta x$ , where  $\delta x$  is the mesh spacing. This indicates that the resolution is only marginal for the Reynolds number chosen

here. However, during the subsequent decay calculation, after several Alfvén times, this excess power at  $k_{Ny}$  disappears, as is seen in Fig. 1 of the Letter.

## Integral scale

The decay of MHD turbulence is characterized by the kinetic and magnetic integral scales. The kinetic integral scale  $\xi_K = k_K^{-1}$  is defined analogously to the magnetic one  $\xi_M = k_M^{-1}$  (given in the Letter), with

$$\xi_K^{-1}(t) = \int_0^\infty k^{-1} E_K(k, t) dk / \mathcal{E}_K(t). \quad (2)$$

Both scales grow in time nearly perfectly proportional to each other like  $t^{1/2}$ ; see Fig. 6. The corresponding decay of kinetic and magnetic energies is proportional to  $t^{-1}$  and is addressed in the next section of this Supplemental Material, where we plot  $u_{rms} = (2\mathcal{E}_K)^{1/2}$  and  $v_A = (2\mathcal{E}_M)^{1/2}$ .

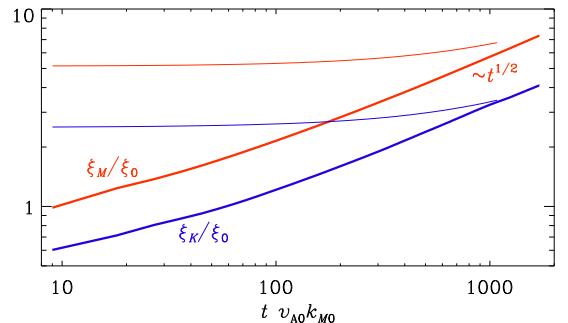


FIG. 6: Kinetic and magnetic integral scales,  $\xi_K$  and  $\xi_M$ , respectively. As in Fig. 4, the thin lines show the result for the  $Pr_M = 10$  run.

## Mach & Alfvén numbers

It has been argued by Kolmogorov that, using the constancy of the Loitsyansky invariant

$$\mathcal{L} = \int r^2 \langle \mathbf{u} \cdot \mathbf{u}' \rangle dr \propto \ell^3 u_\ell^2 \quad (3)$$

with typical velocity  $u_\ell$  on scale  $\ell$ , that, based on dimensional arguments alone, the kinetic energy should decay like  $\mathcal{E}_K \propto \mathcal{L}^{2/5} t^{-6/5}$ . This decay law is confirmed by experiments [6] and simulations, including simulations using the PENCIL CODE [7], both of which suggest a  $t^{-1.25}$  scaling.

This result has been generalized to MHD by Davidson [8], although no numerical confirmation of this has been mentioned in subsequent reviews [9]. On the other

hand, if the decay is governed by viscosity, dimensional arguments suggest  $\mathcal{E}_K \propto \nu t^{-1}$  and  $\ell \propto (\nu t)^{1/2}$ , both of which appear consistent with our simulations. If that is the case, we should expect  $\mathcal{L}$  to grow with time like  $\mathcal{L} \propto \nu^{5/2} t^{1/2}$ .

In the table preliminary table below we give values of  $\mathcal{L}$  (LI) and  $u_{\text{rms}}^2$  for a low resolution run ( $64^3$  mesh points) and a down-sampled one of Run A of the Letter ( $2304^3$  mesh points).

#### $64^3$ run

t	LI	$u^2$
40.6	2.082e-07	7.978e-03
100.0	-5.353e-07	6.965e-05
250.0	-8.427e-07	1.146e-05

#### $2304^3$ run

t	LI	$u^2$
50.0	-4.350e-09	1.027e-04
150.0	-1.067e-08	3.337e-05

The data in the table suggest that  $|\mathcal{L}|$  has a tendency to increase with time. This would support our argument above in favor of viscously dominated decay behavior. On the other hand, as the resolution is increased by a factor of 36,  $\mathcal{L}$  deceases by about two orders of magnitude while  $u_{\text{rms}}$  stays about the same. This would be consistent with  $\mathcal{L}$  converging to zero and therefore not being able to constrain the decay.

In Fig. 7, we plot the Mach number  $u_{\text{rms}}/c_s$ , the Alfvén number  $u_{\text{rms}}/v_A$ , and the ratio  $v_A/c_s$ , where  $u_{\text{rms}}$  and  $v_A$  are the rms values of velocity and magnetic field (density is approximately constant), and  $c_s = \text{const}$  is the isothermal sound speed.

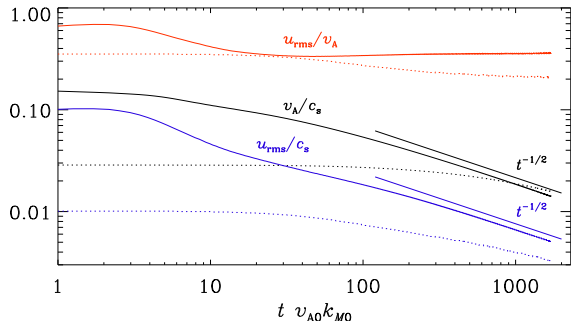


FIG. 7: Mach number  $u_{\text{rms}}/c_s$  (black), Alfvénic Mach number  $u_{\text{rms}}/v_A$  (red), and the ratio  $v_A/c_s$  (blue).

Both  $u_{\text{rms}}$  and  $v_A$  decay in time proportionally to  $t^{-1/2}$ , so the kinetic and magnetic energies decay like  $\mathcal{E}_K(t) = u_{\text{rms}}^2/2 \propto t^{-1}$  and  $\mathcal{E}_M(t) = v_A^2/2 \propto t^{-1}$ . Earlier work [5] resulted in a decay law proportional to  $t^{-0.9}$ , but this departure from the  $t^{-1}$  law is likely a consequence of insufficient scale separation;  $k_0/k_1$  is now 60 compared to 15 previously.

#### Projections onto strain tensor

To examine whether there is a tendency for the turbulence to become locally two-dimensional, we have computed the rate-of-strain tensor,

$$s_{ij} = \frac{1}{2} (u_{i,j} + u_{j,i}). \quad (4)$$

Since  $s_{ij}$  is symmetric, it has three real eigenvalues,  $\lambda_i$  for  $i = 1, 2$ , and 3. They are traditionally ordered such that

$$\lambda_1 < \lambda_2 < \lambda_3. \quad (5)$$

The corresponding eigenvectors are called  $\hat{e}_i$ .

If the flow was incompressible, their sum would vanish, which is here also approximately the case. The largest eigenvalue  $\lambda_3$  corresponds to stretching in the direction  $\hat{e}_3$ , and the most negative one,  $\lambda_1$ , corresponds to compression in the direction  $\hat{e}_1$ .

It has been known for some time [10, 11] that in isotropic turbulence the vorticity vector tends to be aligned with the direction  $\hat{e}_2$  and is therefore normal to the plane where the flow would be two-dimensional. If the turbulence was perfectly two-dimensional, the intermediate eigenvalue of the rate-of-strain tensor would vanish. This is however not the case; see Fig. 8, where we plot probability density functions (PDFs) of the three eigenvalues.

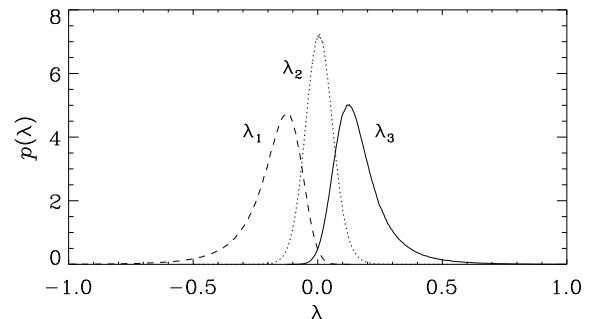


FIG. 8: PDF of the eigenvalues of the rate-of-strain tensor. Note that the intermediate ones are not vanishing, as expected for two-dimensional turbulence.

In the present simulations, we see all the usual characteristics of three-dimensional MHD turbulence where the vorticity vector  $\omega$  is aligned with the eigenvector  $\hat{e}_2$ . Also the magnetic field  $\mathbf{B}$  is aligned with  $\hat{e}_2$ ; see Fig. 9. Here, the PDFs  $p(\cos \phi)$  are normalized such that

$$\int_0^1 p(\cos \phi) d \cos \phi = 1. \quad (6)$$

Furthermore, while  $\omega$  is perpendicular to  $\hat{e}_1$  and  $\hat{e}_3$ , the angle between  $\mathbf{B}$  and both  $\hat{e}_1$  and  $\hat{e}_3$  is about  $45^\circ$  (see

lower panel of Fig. 9), which was first found in MHD shear flows; see Ref. [12], who interpreted their finding as alignment with the direction of the overall shear. In this connection we recall that a shear flow can be decomposed into a rotational and a straining motion [13]. The rotational motion is not captured by the strain tensor. The directions of compression and stretching are then at  $45^\circ$  angles with respect to the direction of the shear [14]. Similar results have recently also been obtained in Ref. [15].

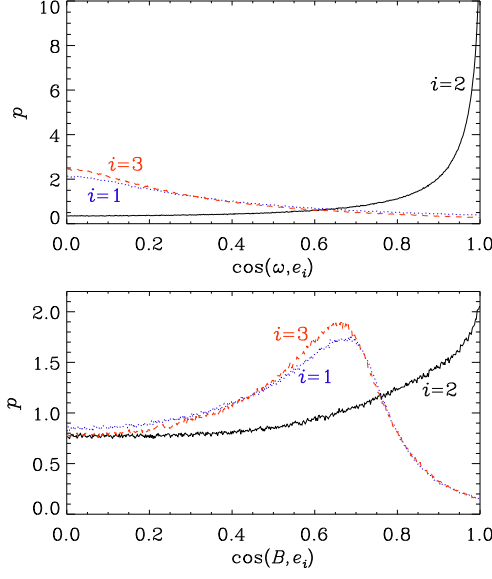


FIG. 9: Alignment of  $\omega$  and  $\mathbf{B}$  with the eigenvectors of the rate-of-strain tensor.

Next, we compute the projections of various vectors  $\sigma$  onto  $s_{ij}$ :

$$s_\sigma = \langle \sigma_i s_{ij} \sigma_j \rangle / \langle \sigma^2 \rangle, \quad (7)$$

where  $\sigma$  is either  $\mathbf{u}$ ,  $\omega$ ,  $\mathbf{B}$ , or  $\mathbf{J}$ . For  $\omega$  and  $\mathbf{B}$ , these values quantify the production of  $\omega$  and  $\mathbf{B}$ , respectively, but for the other quantities no such interpretation exists. In Table II we give the mean and rms values of the  $s_\sigma$ . Here we also compare with the projection of  $\mathbf{A}$  onto the direction  $\hat{\mathbf{e}}_2$ , i.e.,  $\mathbf{A} \rightarrow \hat{\mathbf{e}}_2(\mathbf{A} \cdot \hat{\mathbf{e}}_2)$ , and therefore  $s_A = \langle \lambda_2(\mathbf{A} \cdot \hat{\mathbf{e}}_2)^2 \rangle / \langle (\mathbf{A} \cdot \hat{\mathbf{e}}_2)^2 \rangle$ .

TABLE II: Mean and rms values of the normalized projections  $s_\sigma$  with  $\sigma = \mathbf{u}$ ,  $\omega$ ,  $\mathbf{B}$ , and  $\mathbf{J}$  onto  $s_{ij}$  and a comparison with the value of  $s_A$  defined in the text.

$\sigma$	$\mathbf{u}$	$\omega$	$\mathbf{B}$	$\mathbf{J}$	$\mathbf{A}$
mean	0.009	0.019	-0.001	0.005	0.007
rms	0.145	0.204	0.069	0.064	0.106

Note that  $s_A$  is not particularly small, as one would expect for a locally nearly two-dimensional flow, and is

in fact comparable to all the other terms. The average of  $\langle B_i s_{ij} B_j \rangle / \langle \mathbf{B}^2 \rangle$  is actually the smallest one among them all.

To exclude the possibility of an inverse cascade due to the invariance of  $\langle \mathbf{A}^2 \rangle$  in two dimensions, we appeal again to the similar widths of the PDFs of the intermediate eigenvalue  $\lambda_{2,i}$ , which is close to those of  $\lambda_1$  and  $\lambda_3$ . This suggests that the flow cannot be regarded as locally two-dimensional.

### Constancy of Reynolds and Lundquist numbers

Since  $u_{\text{rms}}$ ,  $v_A$ , and  $k_M$  are all proportional to  $t^{-1/2}$  the decay is self-similar in such a way that the Reynolds and Lundquist numbers,  $\text{Re} = u_{\text{rms}}/\nu k_M$  and  $\text{Lu} = v_A/\eta k_M$ , remain constant. This is clearly demonstrated in Fig. 10, where we plot  $\text{Re}$  (dotted) and  $\text{Lu}$  (solid) both for Runs A and B with  $\text{Pr}_M = 1$  and 10, respectively.

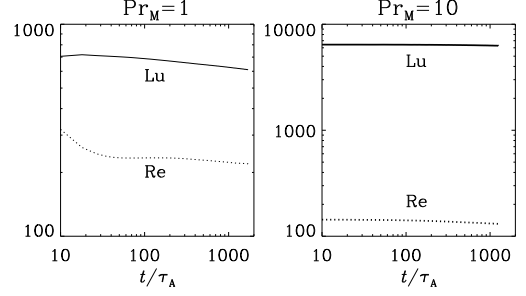


FIG. 10: Instantaneous magnetic and kinetic Reynolds numbers for Runs A and B with  $\text{Pr}_M = 1$  and 10, respectively.

During the decay, the approximate values of  $\text{Re}$  and  $\text{Lu}$  are 230 and 700 for Run A and 130 and 6300 for Run B. As discussed in the Letter, for Run B the value of  $\text{Lu}$  is so huge that, even though we also have a large number of mesh points, one must be concerned about the numerical accuracy of the simulation. One should note, however, that, because  $\text{Pr}_M = 10$  is larger than unity, most of the energy is dissipated viscously. Therefore, although  $\text{Lu}$  is huge, less magnetic energy needs to be dissipated than for  $\text{Pr}_M = 1$ . This was demonstrated first in Ref. [16] for the opposite case with  $\text{Pr}_M \ll 1$  (where Joule dissipation dominates) and later, in Refs. [17, 18], for  $\text{Pr}_M \gg 1$ , which is the case relevant here.

### Energy transfers

In the Letter we considered the spectral transfer function  $T_{kpq} = \langle \mathbf{J}^k \cdot (\mathbf{u}^p \times \mathbf{B}^q) \rangle$ , which governs the gain of magnetic energy and correspondingly the loss of kinetic energy. There is also a kinetic energy transfer

function  $S_{kpq}$ , which describes the transfer between different scales. It vanishes for  $k = p$  and is given by  $S_{kpq} = \rho_0 \langle \mathbf{u}^k \cdot (\mathbf{u}^p \times \boldsymbol{\omega}^q) \rangle$ , where  $\rho_0 = \langle \rho \rangle$  is the average density; compressibility effects have been ignored here. The transfer function  $S_{kpq}$  enters only in the kinetic energy equation. Thus, the magnetic and kinetic energy equations are given by

$$\frac{d}{dt} \left\langle \frac{1}{2} \mathbf{B}_k^2 \right\rangle = T_{kpq} - \eta k^2 \langle \mathbf{B}_k^2 \rangle, \quad (8)$$

$$\frac{d}{dt} \left\langle \frac{1}{2} \rho_0 \mathbf{u}_p^2 \right\rangle = -T_{kpq} - S_{kpq} - \nu p^2 \langle \rho_0 \mathbf{u}_p^2 \rangle. \quad (9)$$

Swapping indices  $k$  and  $p$  in Equation (9) yields

$$\frac{d}{dt} \left\langle \frac{1}{2} \rho_0 \mathbf{u}_k^2 \right\rangle = -T_{pkq} - S_{pkq} - \nu k^2 \langle \rho_0 \mathbf{u}_k^2 \rangle. \quad (10)$$

To get the total energy at wavenumber  $k$ , we now add Equations (8) and (10), i.e.,

$$\begin{aligned} \frac{1}{2} \frac{d}{dt} \langle \mathbf{B}_k^2 + \rho_0 \mathbf{u}_k^2 \rangle &= T_{kpq} - T_{pkq} - S_{pkq} \\ &\quad - \eta k^2 \langle \mathbf{B}_k^2 \rangle - \nu k^2 \langle \rho_0 \mathbf{u}_k^2 \rangle. \end{aligned} \quad (11)$$

The total energy has contributions from all  $p$  and  $q$  and it is of interest to separate between those that are larger and smaller than  $k$ , so we write

$$\begin{aligned} \frac{1}{2} \frac{d}{dt} \langle \mathbf{B}_k^2 + \rho_0 \mathbf{u}_k^2 \rangle &= \Pi_{p \geq k}^{q \geq k} + \Pi_{p \geq k}^{q < k} + \Pi_{p < k}^{q \geq k} + \Pi_{p < k}^{q < k} \\ &\quad - \eta k^2 \langle \mathbf{B}_k^2 \rangle - \nu k^2 \langle \rho_0 \mathbf{u}_k^2 \rangle. \end{aligned} \quad (12)$$

where

$$\Pi_{p > k}^{q < k} = \sum_{p > k} \sum_{q > k} (T_{kpq} - T_{pkq} - S_{pkq}). \quad (13)$$

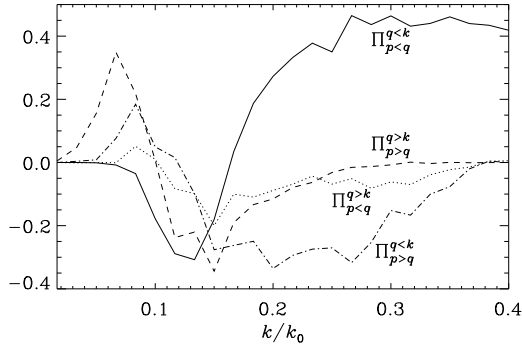


FIG. 11: Energy transfer functions defined in Equation (13).

The results in Fig. 11 show that  $\Pi_{p < k}^{q < k}$  is positive for  $k/k_0 > 0.25$ , demonstrating that there is a gain of total energy at wavenumbers  $k/k_0 > 0.25$  from interactions

with smaller wavenumbers. This shows that there is forward transfer at those wavenumbers. Furthermore, for  $k/k_0 > 0.25$ , the spectral transfer is approximately independent of  $k$ , as expected for a proper forward cascade. There is also a short range  $0.15 < k/k_0 < 0.3$ , where  $\Pi_{p > k}^{q < k}$  is negative. This suggests the existence of inverse transfer resulting from mixed interactions of  $p > k$  and  $q < k$ . In our simulations,  $|T_{kpq}|$  dominates over  $|S_{kpq}|$ , so the dominant contribution to wavenumbers  $q$  comes from the magnetic field.

## Concluding remarks

The decay of magnetically dominated MHD turbulence is a rich field, sharing several similarities with the case in which the magnetic field is dynamo-generated, for example the alignment properties with the eigenvectors of the rate-of-strain tensor. In the Letter, we have focussed on the inverse transfer properties that were previously only known for helical MHD turbulence. This is a new and exciting result that has now been confirmed by two additional independent groups [19, 20].

- 
- [1] A. Brandenburg, T. Kahnashvili, and A. G. Tevzadze, Phys. Rev. Lett., submitted, arXiv:1404.2238 (2014).
  - [2] A. Brandenburg, K. Enqvist, and P. Olesen, Phys. Rev. D **54**, 1291 (1996).
  - [3] T. Kahnashvili, A. Brandenburg, A. G. Tevzadze and B. Ratra, Phys. Rev. D **81**, 123002 (2010).
  - [4] A. G. Tevzadze, L. Kisslinger, A. Brandenburg and T. Kahnashvili, Astrophys. J. **759**, 54 (2012).
  - [5] T. Kahnashvili, A. G. Tevzadze, A. Brandenburg and A. Neronov, Phys. Rev. D **87**, 083007 (2013).
  - [6] H. S. Kang, S. Chester, and C. Meneveau, J. Fluid Mech. **480**, 129 (2003).
  - [7] Haugen, N. E. L., & Brandenburg, A., Phys. Rev. E **70**, 026405 (2004).
  - [8] P. A. Davidson, J. Turb. **1**, 006 (2000).
  - [9] Davidson, P. A., J. Fluid Mech. **663**, 268 (2010).
  - [10] R. M. Kerr, J. Fluid Mech. **153**, 31 (1985).
  - [11] W. T. Ashurst, A. R. Kerstein, R. M. Kerr, C. H. Gibson, Phys. Fluids **30**, 2343 (1987).
  - [12] A. Brandenburg, Å. Nordlund, R. F. Stein, and I. Torkelsson, Astrophys. J. **446**, 741 (1995).
  - [13] Brandenburg, A., Chaos, Solitons & Fractals **5**, 2025 (1995).
  - [14] A. Brandenburg, R. L. Jennings, Å. Nordlund, M. Rieutord, R. F. Stein, and I. Tuominen, J. Fluid Mech. **306**, 325 (1996).
  - [15] S. Sur, L. Pan, and E. Scannapieco, arXiv:1406.0859 (2014).
  - [16] A. Brandenburg, Astrophys. J. **697**, 1206 (2009).
  - [17] Brandenburg, A., Astron. Nachr. **332**, 51 (2011).
  - [18] A. Brandenburg, Astrophys. J. **791**, 12 (2014).
  - [19] A. Berera and M. Linkmann, arXiv:1405.6756 (2014).
  - [20] J. Zrake, arXiv:1407.5626 (2014).